Quantification of Stern Layer Water Molecules, Total Potentials, and Energy Densities at Fused Silica:Water Interfaces for Adsorbed Alkali Chlorides, CTAB, PFOA, and PFAS

HanByul Chang, Emilie H. Lozier, Emily Ma, and Franz M. Geiger*

Department of Chemistry, Northwestern University, 2145 Sheridan Road,

Evanston, Illinois 60208, United States

ABSTRACT. We have employed amplitude and phase resolved second harmonic generation spectroscopy to investigate ion specific effects of monovalent cations at the fused silica:water interface maintained at acidic, neutral, and alkaline conditions. We find a negligible dependence of the total potential (as negative as -400 mV at pH 14), the second order nonlinear susceptibility (as large as 1.5 x 10^{-21} m^2 V^{-1} at pH 14), the number of Stern layer water molecules (1 x 10^{15} cm^{-2} at pH 5.8), and the energy associated with water alignment upon going from neutral to high pH (*ca*. -24 kJ mol^{-1} to - 48 kJ mol^{-1} at pH 13 and 14, close to the cohesive energy of liquid water but smaller than that of ice) on chlorides of the alkali series (M^+=Li^+, Na^+, K^+, Rb^+, and Cs^+). Attempts are presented to provide estimates for the molecular hyperpolarizability of the cations and anions in the Stern layer at high pH, which arrive at *ca*. 20-fold larger values for $\alpha^{(2)}_{total\ ions} = \alpha^{(2)}_{M^+} + \alpha^{(2)}_{OH^-} + \alpha^{(2)}_{Cl^-}$ when compared to water's molecular hyperpolarizability estimate from theory and point to a sizable contribution of deprotonated silanol groups at high pH. In contrast to the alkali series, a pronounced dependence of the total potential and the second order nonlinear susceptibility on monovalent cationic (cetrimonium bromide, CTAB) and anionic (perfluorooctanoic and perfluorooctane sulfonic acid, PFOA and PFOS) surfactants was quantifiable. Our findings are consistent with a low surface coverage of the alkali cations and a high surface coverage of the surfactants. Moreover, they underscore the important contribution of Stern layer water molecules to the total potential and second order nonlinear susceptibility. Finally, they demonstrate the

applicability of heterodyne detected second harmonic generation spectroscopy for identifying perfluorinated acids at mineral:water interfaces.

*Corresponding author: f-geiger@northwestern.edu

I. Introduction. The transport and interactions of alkali metals at mineral surfaces[1] are important for various natural processes and industrial applications ranging from biological[2-5] and environmental[6] chemistry to energy storage[7-9] and electrochemistry.[10] Despite this general importance and relevance, the quantification of interfacial structure and electrostatics for the alkali halides has been hampered by the fact that there are only a few label-free and surface-selective experimental probes that are ion-specific.[11-15] Among them are X-ray spectroscopies, which can track the exchange of alkali cations on various mineral substrates such as muscovite mica, but require a synchrotron source.[16] Ion-specific electrodes sample far from the Stern layer and therefore lack surface-selectivity, even though they are a powerful means for acquiring spatially resolved information.[10] Related techniques used to study interfacial interactions range from bulk titration techniques,[17] scanning probes and microscopies,[13-15, 18, 19] neutron diffraction,[11] atomistic simulations,[20-24] to spectroscopic techniques,[25] including nonlinear optics, such as second harmonic generation (SHG).[26-28] Because SHG only occurs in symmetry-breaking environments, the phenomenon can provide information about structure and electrostatics at the boundary between two media (i.e., water, fused silica), using a relatively straightforward table-top spectroscopic setup. The approach provides some advantages over other surface-sensitive techniques that require alterations of the sample itself or the surrounding environment of the reaction.

In this context, we set out to determine whether heterodyne-detected second harmonic generation (HD-SHG) spectroscopy is conducive to adding structural and electrostatic information to the field of interfacial ion-specific effects for monovalent ions. We are motivated by our recent reports of clear ion-specific signatures in the second-order nonlinear susceptibility, $\chi^{(2)}$, and the total potential, $\Phi(0)_{tot}$, at the fused silica:aqueous interface in the presence of divalent *versus* monovalent ions,[29, 30] but expect these signatures to be much fainter, if detectable at all, for monovalent ions, given their low propensity to bind to the silica surface when compared to di- or even trivalent ions.

Given a large amount of information available on ion-specific effects from electrokinetic measurements,[31] X-ray spectroscopy,[32-34] as well as atomistic simulations[20-24, 35, 36] on fused silica:aqueous interfaces, we study the fused silica:water interface at several selected pH values and ionic strengths using the alkali chlorides, LiCl, KCl, NaCl, RbCl, and CsCl. We hypothesize that even though the cations have different hydration chemistries, hyperpolarizabilities, and sizes, the ions' surface coverages are not high enough to result in distinguishable ion-specific outcomes in $\chi^{(2)}$ and $\Phi(0)_{tot}$. We base our hypothesis on X-ray spectra reported by Duval et al.,[37] which show that approximately 85% of SiO_2's surface sites do not participate in amphoteric chemistry. In other words, about 85% of the surface sites remain neutral SiOH groups, irrespective of the bulk solution pH. While these neutral sites are poor monocation binders, they contribute to the overall $\chi^{(2)}$ values and can be accounted for by referencing to the $\chi^{(2)}$ value obtained at pH 2, close to the point of zero charge (PZC),[38-41] as we will show later.

We express the second-order nonlinear susceptibility as a sum of its constituents, from approximately more to less abundant at the interface, according to $\chi^{(2)} = \chi^{(2)}_{H_2O} + \chi^{(2)}_{SiOH} + \chi^{(2)}_{SiO^-} + \chi^{(2)}_{SiOH_2^+} + \chi^{(2)}_{M^+} + \chi^{(2)}_{X^-}$. Here, M^+ refers to the cation and X^- refers to the counter anion. To leading

order, the $\chi^{(2)}_{SiOH}$ term and the nonlinear susceptibility of the Stern layer water molecules hydrogen-bonded to the silanol groups remain constant for each solution condition (as mentioned above, the surface chemistry is dominated by the ~85% neutral SiOH groups and the silanol groups cannot flip their absolute orientation). For conditions of high pH, where the number of protonated silanol groups and counter anions is negligible, we find that the changes in the overall $\chi^{(2)}$ should be due to changes in $\chi^{(2)}_{M^+}$, $\chi^{(2)}_{SiO^-}$, and the $\chi^{(2)}_{H_2O}$ of the water molecules associated with the SiO^- and adsorbed M^+ species. Given the small number of deprotonated silanol groups even at elevated pH (~15%), we expect no significant changes in the overall $\chi^{(2)}$ for our alkali chlorides. However, we expect surfactants such as cetrimonium bromide (CTAB) or perfluorooctanoic acid (PFOA) and perfluorooctane sulfonic acid (PFOS)–with the same monovalent charge but significantly higher number of polarizable electrons along the carbon tail and larger surface coverage–to elicit large, distinguishable differences in $\chi^{(2)}$ and $\Phi(0)_{tot}$ relative to the alkali cations. We also chose these species due to their environmental[42] and technological relevance[43-47] and specifically due to CTAB's versatility of adopting multiple morphologies at interfaces that range from monomers to micelles to bilayers to adlayers.[48-52]

II. Experimental. In the experiments, we employ HD-SHG[53] spectroscopy. The method yields the SHG electric field amplitude, E_{sig}, and phase, φ_{sig}, from which the total interfacial potential, $\Phi(0)_{tot}$, and the second order nonlinear optical susceptibility, $\chi^{(2)}$, are readily obtained according to[6, 29, 54-63]

$$\Phi(0)_{tot} = -C \times \frac{E_{sig}\sin(\varphi_{sig})}{\chi^{(3)}_{water}\{cos(\varphi_{DC})\sin(\varphi_{DC})+1.5\}} \quad (1)$$

$$\chi^{(2)} = C \times \left(E_{sig}\right)\cos\left(\varphi_{sig}\right) + \Phi(0)_{tot}\,\chi^{(3)}_{water}\cos^2(\varphi_{DC}) \quad (2)$$

For our fused silica hemispheres, the calibration factor C is $3.6 \times 10^{-22} m^2 V^{-1}$ in our spectrometer,[64] measured by taking the ratio of the SHG responses from the substrate:ultrapure water (18.2 MΩ ·cm, 2 mM ionic strength, and pH 5.8) interface and an aligned piece of z-cut α-quartz as an external IEEE phase reference standard[65, 66] with known $\chi^{(2)}_{Bulk,Q} = 8 \times 10^{-13}$ m V^{-1} in place of the water while properly accounting for Fresnel coefficients.[67, 68] The third-order susceptibility of water, $\chi^{(3)}_{water}$, stems from water molecules in the diffuse layer of the EDL and is estimated to be $1 \times 10^{-21}\ m^2\ V^{-2}$ from experiment and theory.[69, 70] This quantity is invariant with ionic strength, pH, and surface composition, so we employ it here. The DC optical phase angle, φ_{DC}, is given by $arctan(\Delta k_z \lambda_D)$,[60, 64, 71] where λ_D is the Debye length (computed from Debye-Hückel theory) and Δk_z is the wave vector mismatch ($1.1 \times 10^7\ m^{-1}$in our spectrometer for $\omega = 1030\ nm$ and $2\omega = 515\ nm$).

$\Phi(0)_{tot}$ is a function of the surface charge, the solution's ionic strength, the Stern layer's relative permittivity and capacitance, and other parameters commonly used in the mean field models describing surface potential, such as the Gouy-Chapman-Stern model. In addition, $\Phi(0)_{tot}$ includes other contributions to the total electrostatic potential drop across the solid:aqueous interface, such as dipole and higher-order contributions,[72] which we recently reported to be up to 90% of the total interfacial potential when compared to the estimate from Gouy-Chapman-Stern theory. $\chi^{(2)}$ contains information on the Stern layer at the fused silica:aqueous interface, comprising SiOH, $SiOH_2^+$, SiO^-, any adsorbed counterions, and water molecules.[73] As a fundamental structural property of noncentrosymmetric matter, $\chi^{(2)}$ depends on the identity and orientation of all species in the Stern layer.[74, 75] In contrast, the third-order $\chi^{(3)}$ term originates from water molecules in the diffuse layer,[76] which forms in response to the DC-field emanating from the charged surface.[63, 77, 78] HD-SHG spectroscopy specifically leverages the phase shift in the $\chi^{(3)}$ term with respect to $\chi^{(2)}$

("$e^{i\varphi_{DC}}$") to separate the contributions from the Stern and diffuse layers.[57] The process of separating these two contributions is now well-understood.[27, 54, 57]

II.A. Laser System. We described our HD-SHG laser setup in detail in our previous work.[26, 54, 57] Briefly, we use a 200-fs pulse laser system (Pharos, Light Conversion, 200 kHz repetition rate, 1030 nm) to conduct our HG-SHG experiments. A Glan-Taylor polarizer (Thorlabs, GT-10) sets the input beam polarization perpendicular to the plane of incidence (*s*-polarized) and a half-waveplate (Thorlabs, AHWP05M-980) attenuates the power to 40 mW. A silver off-axis parabolic (OAP) mirror recollimates the reflected fundamental beam and SHG ("output beam") in space using and a calcite time-delay compensator (Newlight Photonics, CAL12200-A) ensures temporal overlap of the beams. The setup achieves interference between the reflected fundamental beam and SHG from the sample by translating a 50-μm-thick z-cut α-quartz window (Precision Micro-Optics, PWQB-368252) – acting as the source of a local oscillator (LO) – along a 100-mm path. Steering mirrors direct the output beam through a shortpass filter and bandpass filter to remove the fundamental beam and finally to a photomultiplier tube (Hamamatsu H8259-01 PMT). We detect the signal using a gated photon counter (Stanford Research Systems, SR400) with a gate width of 50 ns.

II.B. Sample, Sample Cell, and Solution Preparation. We prepared our fused silica hemispheres by first soaking them in a solution of ALNOCHROMIX (Alconox Labs) and concentrated sulfuric acid (Sigma-Aldrich, 339741, 99.999%) for 1 hour. We then rinsed the hemisphere with water, sonicated in methanol and water for 15 minutes each, and subsequently stored the clean substrate in ultrapure water (18.2 MΩ·cm, MilliporeSigma) until use. Before each use, we sonicated the hemisphere in methanol and water for 15 minutes, each, again. After water sonication, we dried the hemisphere using house N_2 gas and plasma cleaned it on the "high" RF setting for ~30 sec.

Before each use, we cleaned our custom-built PTFE cell sample cell by sonicating in methanol and water for 15 minutes each. We rinsed the cell with copious amounts of ultrapure water between each sonication. After water sonication, we dried the cell with N_2 and plasma cleaned it on high RF for ~30 seconds. We rinsed our fluoroelastomer O-rings with methanol using a squeeze bottle and rinsed with copious amounts of ultrapure water. We assembled the sample cell and filled it with ultrapure water before mounting the hemisphere, to ensure the fused silica surface was always in contact with water.

By flushing the tubing for the peristaltic pump system with water for 30 minutes before and after each day's experiments and using fresh tubing for each salt, we minimized cross-contamination. After optical alignment, we left the system to equilibrate for 2 hours, during which ultrapure water flowed continuously through the system at 2 mL min^{-1}.

All salt solutions were prepared by dissolving the appropriate amount of salt in ultrapure water (18.2 MΩ·cm, MilliporeSigma) and left to equilibrate with atmospheric CO_2 overnight. The salts and surfactants used for this work are as follows: NaCl (Sigma-Aldrich, 746398, ≥ 99%), KCl (Thermo Fisher Scientific, BP366, > 99.0 %), LiCl (Sigma-Aldrich, 793620, > 99%), CsCl (Sigma-Aldrich, C3011, ≥ 99.0%), RbCl (Sigma-Aldrich, R2252, ≥ 99.0%), CTAB (Sigma-Aldrich, H6269, ≥ 99%), PFOA (Sigma-Aldrich, 171468, 95%) and PFOS (Sigma-Aldrich, 77282, ≤98.0%). We used individual solutions for up to three days. We prepared pH 2 and 10 solutions immediately before use and used solutions for pH 5.8 experiments without any pH adjustments. In cases were solutions required pH adjustment, we used concentrated 1 M HCl or hydroxides of the corresponding salt. We prepared 1 M solutions at pH 14 by dissolving pure hydroxides of each salt directly in the water and measuring out the mass of salts needed to achieve a total ionic strength of 1 M. After preparing these solutions, we did not adjust the pH further and typically, the pH

reading was 14.5 ± 2. For simplicity we will refer to these solutions as "pH 14 solutions" hereafter. The salts used to make pH 14 solutions are as follows: NaOH (Millipore Sigma, SX0590, < 99%), KOH (Sigma-Aldrich), LiOH (Sigma-Aldrich, 442410, 98%), RbOH (Sigma-Aldrich, 243892, 99.9%), and CsOH (Sigma-Aldrich, 232041, 99.9%). Table I lists the solution conditions employed here.

II.C. Data Collection. After the 2-hour stabilization period, we recorded four replicate HD-SHG scans of the fused silica:water interface to obtain the reference amplitude and phase. Each scan was completed within 20 seconds and each scan occurred every minute, accounting for the time for the translational stage to move back to the starting position. We then changed the solution to the target pH and ionic strength for a given experiment and flowed the solution at 2 mL min^{-1} for 30 minutes before recording four replicate HD-SHG scans. We obtained the phase shift and intensity by fitting the interference patterns to a trigonometric function of the form $y = a + E_{sig}\cos(kx + \varphi_{sig})$ where a is an intensity offset, E_{sig} is the SHG amplitude, k is the period for our translational stage, x is the stage position, and φ_{sig} is the SHG phase.[53]

III. Results and Discussion.

III.A. No Pronounced Ion Specificity (Li to Cs) in Interfacial Structure, Electrostatics, or Energy Densities. Fig. 1 shows the $\chi^{(2)}$ values obtained from our HD-SHG measurements. Positive $\chi^{(2)}$ values are understood to report on an "up" orientation where most of the Stern layer water molecules point their oxygen atoms into the bulk electrolyte while negative values correspond to water molecules' oxygen atoms pointing towards the surface. This result recapitulates our earlier finding of purely positively signed $\chi^{(2)}$ values for pH 1 to 12 at 0.5 M ionic strength [NaCl)[64] to the other alkali cations.

Fig. 1 also shows the total surface potentials, which are generally consistent with our earlier reported results using just NaCl: The total potential changes from slightly positive at pH 2 (below the PZC) to around – 400 mV at high pH. At pH 5.8, the total potentials are more negative at low ionic strength when compared to high ionic strength at the same pH. As we reported earlier,[64] the total interfacial potential drop across the EDL that we quantify here contains the Gouy-Chapman-Stern plus the dipolar and multipolar (non-GCS) potentials and their cross-interactions (ion-dipole etc.). Independent measurements using electrical impedance spectroscopy[41, 79, 80] and X-ray-based techniques [81] that also provide the total potential drop across the solid:electrolyte interface fully validate these findings.

Overall, we find that the presence of the alkali cations studied here does not lead to distinguishable changes in $\Phi(0)_{tot}$, likely for the same reason that ion-specific outcomes are only minor, if undetectable, in $\chi^{(2)}$. As we reported recently,[72] the total potentials we obtain using NaCl are significantly larger (50% at low ionic strength, 90% at high ionic strength) in magnitude when compared to the result from Gouy-Chapman-Stern theory. The same holds here as well for the various alkali cations surveyed, given the similarity in total surface potentials seen in Fig. 1. Considering the full dataset in Fig. 1, we conclude that neither $\chi^{(2)}$ nor the total potential exhibit a marked dependence on the choice of alkali cation. This result is in contrast to the marked difference in both of these surface properties when comparing monovalent NaCl with divalent $MgSO_4$ at the fused silica:water interface.[26]

In an attempt to isolate any ion-specific signature in $\chi^{(2)}$, we show in Fig. 2 the $\Delta\chi^{(2)}$ values we obtained by subtracting from each $\chi^{(2)}$ value shown in Fig. 1 the $\chi^{(2)}$ value obtained from the fused silica:water interface at pH 2 and 100 mM ionic strength (this value is ~$1 \times 10^{-22}\ m^2\ V^{-1}$, depending on the cation). We employ this reference condition as it is close to the PZC. The method

effectively subtracts the net-neutral background contribution from the fused silica:water interface to $\chi^{(2)}$. We apply it only to the high salt concentrations (100 mM and 1 M) in the dataset shown in Fig. 1. Again, we do not find a marked ion-specific outcome in the $\Delta\chi^{(2)}$ values. These findings are generally consistent with Hofmeister-type nonlinear optical measurements at the fused silica:water interface, such as those of the Gibbs[82-84] or Cremer groups.[85]

In a further attempt to discern ion-specific effects on the energetics associated with net-aligned Stern layer water molecules at high pH – where we would expect the highest cation surface coverage and thus an ion-specific outcome – we estimated the number of net-aligned Stern layer water molecules at that high pH. To this end, we divided the high-pH $\Delta\chi^{(2)}$ values by the average of molecular hyperpolarizability point estimates for liquid water from experiment[86] and electronic structure theory by Gubskaya and Kusalik[87] that other groups have used successfully to compute non-resonant third-order nonlinear properties of the electrical double layer under non-resonant conditions[70] that match the experimentally determined value for aqueous interfaces to within 10%.[69] The mean second-order molecular hyperpolarizability appears to be dominated by the zzz-tensor element[87] to which we are most sensitive. Gubskaya and Kusalik provides detailed tables containing estimates from electronic structure calculations of the three relevant tensor elements (zxx, zyy, and zzz) of water's molecular hyperpolarizability, along with a mean value, computed according to Maroulis.[88] The mean accounts for averaging over many orientations in an isotropic liquid, which is necessary for computing the third-order nonlinear susceptibility as reported by Lütgebaucks, Gonella, and Roke in the Supporting Information of their Phys. Rev. B paper.[70] That paper uses a molecular hyperpolarizability value of 3.09×10^{-52} C m^3 V^{-2}, citing the Gubskaya and Kusalik paper (even though the mean molecular hyperpolarizabilities listed in the Tables of Gubskaya and Kusalik are computed to be about three times larger). Unlike the water molecules

in the diffuse layer, the Stern layer water molecules are of course located in an asymmetric environment, as pointed out by Lütgebaucks, Gonella, and Roke,[70] with our polarization combination probing largely the zzz tensor element of the hyperpolarizability. Gubskaya and Kusalik's calculations show that the mean hyperpolarizability is close in value to the zzz tensor element at various levels of theory (up to MP4) and types of models they used for liquid water.[87] Gubskaya and Kusalik actually cite an experimental study of the second-order molecular hyperpolarizability of pure liquid water published by Levine and Bethea,{Levine, 1976 #15032} who presumably used the same psec YAG laser they used in their 1974 study of pure organic liquids (close to the same wavelength as our LightConversion Flint oscillator, even though the Levine and Bethea paper contains no experimental details to that effect, sadly - yet, their preceding papers mention a YAG laser). Assuming a YAG laser was used, Levine and Bethea's experiment yields a second-order molecular hyperpolarizability of pure liquid water of 0.46 x 10^{-31} e.s.u., or 1.71 x 10^{-52} C m^3 V^{-2} (±15%), which should be applicable to our 1030 nm laser wavelength as well. This value is three times smaller than the one we used in our eqn. 3, for which we employed the average of the experimental (Levine and Bethea) and electronic structure theory (Gubskaya and Kusalik) estimate. Now, we take this average value,$\alpha^{(2)} = 5.3 \times 10^{-52}\ C\ m^3\ V^{-2}$), and assume it to be applicable to the net-aligned Stern layer water molecules, i.e. their zzz-tensor elements, at least to leading order. We then obtained the number of net-aligned water molecules per cm^2 by accounting for the Stern layer water permittivity (ε=1.77 to 2)[89], according to

$$N_{\uparrow} = \Delta\chi^{(2)}\varepsilon\varepsilon_o\left(10^4 cm^2 m^{-2}\alpha^{(2)}\right)^{-1} \qquad (3),$$

where ε_o is the vacuum permittivity (the upwards arrow indicates water's oxygen pointing towards the aqueous phase and its protons pointing towards the surface; we assume the alkali cation contribution to be small, given the small surface coverages of SiO^- groups).

Fig. 2 shows no discernable ion-specific outcomes in the number of net-aligned Stern layer water molecules, at least within the uncertainties of our point estimates (errors were appropriately propagated).[90] At pH 5.8 and 100 mM ionic strength, we find that eqn. 3's estimate for the number of net-aligned water molecules in the interfacial region (~1 x 10^{15} cm^{-2}) matches the calculated estimate for a 1 cm^2 area of liquid water at standard temperature and pressure (1.04 x 10^{15} cm^{-2}). Given that ~85% of the surface consists of (neutral) SiOH groups at this pH, a net protons-down water alignment of would seem to indicate that the majority of Stern layer water molecules are hydrogen bond donors (to the silanol oxygen atoms) at pH 5.8.

At high pH, eqn. 3 predicts a ca. three- to five-fold increase in the number of water molecules in the interfacial region, suggesting perhaps a widening of the Stern layer as the pH is raised. However, we caution that eqn. 3 should be expanded to include the hyperpolarizabilities of the adsorbed cations and anions at elevated pH (unlike in our initial assumption at circumneutral pH), in addition to that of the Stern layer water molecules. Complicating the situation is that this premise assumes that the Stern layer relative permittivity is pH invariant, which is probably not the case. Li is the only alkali cation with fewer electrons (2) than water or hydroxide (10), and the chloride counter ion has 7 more electrons than the water molecules and hydroxide ions. These species save Li^+ should therefore have a larger nonlinear molecular hyperpolarizability and second-order nonlinear susceptibility than the interfacial water molecules that should be accounted for. Subtracting the pH 5.8/100 mM $\Delta\chi^{(2)}$ value (due to the net-aligned Stern layer water molecules) from the high pH values results in $\Delta\Delta\chi^{(2)}$ point estimates that would be associated with the ions in the interfacial region (mainly the cations in the outer Helmholtz plane and the hydroxide, and chloride ions in the diffuse layer). Fig. 3 shows that the magnitude of the propagated uncertainties associated with the point estimates does not allow us to discern ion specific outcome

in this analysis either, as perhaps expected given the arguments presented above. Yet, our estimations seem to indicate that at high pH, the cations and anions in the double layer have a collective second-order nonlinear susceptibility (~1 x 10^{-21} m^2V^{-1}) that is 3 to 5 times larger than that of the Stern layer water molecules identified at pH 5.8/100 mM ionic strength (2 x 10^{-21} to 5 x 10^{-21} m^2V^{-1}). Dividing this point estimate of (~1 x 10^{-21} m^2V^{-1} by the 15% of negatively charged sites (0.15 x 10^{15} cm^{-2}) from the XPS measurements by Ehrhardt et al. yields a "collective molecular hyperpolarizability" of the cations and anions in the double layer, $\alpha^{(2)}_{ions}$ in the range of 1 x 10^{-50} C m^3 V^{-2} (computed by rearranging eqn. 3), ca. 20 times larger than the molecular hyperpolarizability we used above ($\alpha^{(2)} = 5.3 \times 10^{-52}\ C\ m^3\ V^{-2}$).[87] Using a larger deprotonated fraction (30% from Gmür et al.,[91] or Dove and Craven)[92] still results in a ten-fold larger hyperpolarizability for the ions than the Stern layer water molecules. More likely is a pH-dependent change in the second-order nonlinear susceptibility of the silica surface, which recent experimental and theory work by the Gibbs group has shown to increase considerably in magnitude with deprotonation state of the surface.[93]

Given our estimate of ~ 1 x 10^{15} net-oriented Stern layer water molecules cm^{-2} at pH 5.8, and assuming that this number does not change appreciably at high pH, we can estimate the energy density (in J cm^{-2}) associated with increasing the pH to 13 or 14 by multiplying this point estimate by the elementary charge, e, and the total interfacial potential (from eq. 1 and Fig. 1) according to

$$E = N_{\uparrow} e\, \Phi(0)_{tot} \qquad (4).$$

Fig. 3 shows the results, which correspond, at pH 13 and 14, to a molar energy density of ~-0.5 x 10^{-4} J cm^{-2} x Avogadro's number / (1 x 10^{15} water molecules cm^{-2}) = -24 kJ mol^{-1} to -48 kJ mol^{-1}. This estimate range includes the cohesive energy of liquid water (44.5 kJ mol^{-1})[94] but not that of ice (59 kJ mol^{-1}).[95] Overall, the general lack of ion-specific outcomes on the various surface

properties we investigated is consistent with a small surface site density (~15%) of deprotonated SiO^- groups to which the alkali cations can bind. The surface properties we surveyed, then, are dominated by the Stern layer water molecules and neutral silanol sites that constitute most surface species to which SHG is sensitive.

III. B. Surfactant Cations and Anions Considerably Change $\chi^{(2)}$ and $\Phi(0)_{tot}$. To test our hypothesis that the ions' surface coverages are too small to observe ion-specific outcomes in the interfacial structure and electrostatics, we added the cationic surfactant CTAB and the anionic surfactants PFOA and PFAS to the aqueous solution. These molecular ions are still monovalent but their well-known surface activity results in a higher surface coverage when compared to the alkali cations. One driving force for adsorption is the ~2.5 kJ mol^{-1} favorable interaction energy for each of the methylene groups that form the hydrocarbon tail of these species. We expect a positive total surface potential for CTAB and a negative total surface potential for the perfluoroalkyl species.

Fig. 3 shows that upon introducing 1 mM CTAB (near the critical micelle concentration at this pH and ionic strength)[96] to a pH 5.8 aqueous solution (no extra ions added), the second-order nonlinear susceptibility and the total potential are oppositely signed when compared to the alkali cations at the same ionic strength and pH. We observed this charge reversal for a polycation before,[97] but only in the SHG phase. The flip in the signs is also evident in the HD-SHG interference patterns shown in Figure 3B. The flip of the total potential and the second-order nonlinear susceptibility is consistent with Stern layer water flipping, as high CTAB concentrations cause fused silica to become overcharged.[52, 54, 98-100] Addition of 24 μM PFOA or 20 μM PFOS (both 10 ppm), which are monovalent anions, results in total potential and the second-order nonlinear susceptibility values that are comparable to those observed for the alkali chlorides (*n.b.*,

the low concentration was chosen so as to have little influence on the bulk solution pH; yet, PFOA addition brough the initial pH of ultrapure water from 5.8 to 4.6, see Table I). The differences in the nonlinear susceptibility and the total potential between PFOA and PFOS are likely due to differences in their respective surface coverages, given the similarity in their structure. A conclusion would then be that PFOS is more surface active than PFOA under the conditions of the experiment (pH 5.8, de-ionized water with 1.2 μS cm^{-1}, 10 ppm perfluorinated compound). We note that a full exploration of how the total potential and the second order nonlinear susceptibility change with varying conditions of surfactant concentration, total ionic strength, and pH is beyond the scope of this present work but certainly within the realm of future investigations.

While the observation that the perfluorinated anions adsorb to the fused silica surface at pH 5.8 (well above the PZC) may be counterintuitive given Coulomb's law, recall that the ~85% neutral SiOH groups dominate fused silica's surface chemistry (*vide supra*). It is likely that PFOA and PFOS adsorb to these neutral SiOH groups through a combination of hydrogen bonding and the favorable hydrophobic interactions (dispersion) among the perfluorinated alkyl tails. Vibrational sum frequency spectroscopy would be an appropriate tool to discern if the surfactants entirely displace all the Stern layer water molecules. A study recently published[101] for CTAB on c-cut sapphire at high pH indicates that interfacial water is displaced at ~4 times lower CTAB concentrations compared to the 1 mM CTAB concentration used here. We therefore cannot use eqn. 3 and our $\Delta\chi^{(2)}$ trick to estimate the number of water molecules in the interfacial region, as we do not yet have an $\alpha^{(2)}$ estimate for the adsorbed surfactants, nor can we provide energy density estimates for the Stern layer for the surfactants yet.

IV. Conclusions. In conclusion, we have employed amplitude and phase resolved second harmonic generation spectroscopy to investigate ion specific effects of monovalent cations at the

fused silica:water interface. We found a negligible dependence of the estimated total potential (as negative as -400 mV at pH 14), the second order nonlinear susceptibility (as large as 1.5 x 10^{-21} m^2 V^{-1} at pH 14), the number of Stern layer water molecules (1 x 10^{15} cm^{-2} at pH 5.8), and the energy associated with water alignment upon going from neutral to high pH (-24 kJ mol^{-1} to -48 kJ mol^{-1}). Attempts were presented to provide estimates for the molecular hyperpolarizability of the cations and anions in the Stern layer at high pH, which arrive at *ca*. 20-fold larger values for $\alpha^{(2)}_{total\ ions} = \alpha^{(2)}_{M^+} + \alpha^{(2)}_{OH^-} + \alpha^{(2)}_{Cl^-}$ when compared to water's molecular hyperpolarizability estimate from theory. The energy density estimate at high pH points to a picture of the Stern layer whose energetics are more comparable to liquid water than that of ice, based on their respective cohesive energies. A pronounced dependence of the first two properties on monovalent cationic and anionic surfactants (CTAB and PFAs) was quantifiable. Our findings are consistent with a low surface coverage of the alkali cations and a high surface coverage of the surfactants. Moreover, they underscore the important contribution of Stern layer water molecules to the total potential and second order nonlinear susceptibility. Finally, they demonstrate the applicability of heterodyne detected second harmonic generation spectroscopy for identifying perfluorinated acids at mineral:water interfaces with a straight-forward non-resonant nonlinear optical method.

V. Acknowledgement. This work was supported by the US National Science Foundation (CHE-2153191), the Air Force Office of Scientific Research (FA9550-16-1-0379), and the Department of Energy (DE-SC0023342). EHL acknowledges a Buffett Global Impacts Graduate Fellowship from the Roberta Buffett Institute for Global Affairs at Northwestern University. FMG designed the experiment. HC, EM, and EHL carried out the experiments. HC, EM, EHL, and FMG analyzed the data and wrote the manuscript.

References.

1. Bañuelos, J. L.; Borguet, E.; Brown Jr, G. E.; Cygan, R. T.; DeYoreo, J. D.; Dove, P. M.; Gaigeot, M.-P.; Geiger, F. M.; Gibbs, J. M.; Grassian, V. H.; Ilgen, A. G.; Jun, Y.-S.; Kabengi, N.; Katz, L.; Kubicki, J. D.; Lützenkirchen, J.; Putnis, C. V.; Remsing, R. C.; Rosso, K. M.; Rother, G.; Sulpizi, M.; Villalobos, M.; Zhang, H., Oxide–and Silicate–Water Interfaces and Their Roles in Technology and the Environment. *Chem. Rev.* **2023,** *123*, 6413-6544.
2. Mähler, J.; Persson, I., A Study of the Hydration of the Alkali Metal Ions in Aqueous Solution. *Inorganic Chemistry* **2012,** *51* (1), 425-438.
3. Ikeda, T.; Boero, M., Communication: Hydration structure and polarization of heavy alkali ions: A first principles molecular dynamics study of Rb+ and Cs+. *The Journal of Chemical Physics* **2012,** *137* (4), 041101.
4. Zhang, C.; Raugei, S.; Eisenberg, B.; Carloni, P., Molecular Dynamics in Physiological Solutions: Force Fields, Alkali Metal Ions, and Ionic Strength. *Journal of Chemical Theory and Computation* **2010,** *6* (7), 2167-2175.
5. Yang, Z.; Li, Q.; Chou, K. C., Structures of Water Molecules at the Interfaces of Aqueous Salt Solutions and Silica: Cation Effects. *J. Phys. Chem. C* **2009,** *113* (19), 8201-8205.
6. Schaefer, J.; Gonella, G.; Bonn, M.; Backus, E. H. G., Surface-specific vibrational spectroscopy of the water/silica interface: screening and interference. *Phys. Chem. Chem. Phys.* **2017,** *19* (25), 16875-16880.
7. Jeon, J.; Cho, M., Ion Transport in Super-Concentrated Aqueous Electrolytes for Lithium-Ion Batteries. *The Journal of Physical Chemistry C* **2021,** *125* (43), 23622-23633.
8. Heath, J. J.; Kuroda, M. A., First principles studies of the interactions between alkali metal elements and oxygen-passivated nanopores in graphene. *Physical Chemistry Chemical Physics* **2018,** *20* (40), 25822-25828.
9. Larcher, D.; Tarascon, J. M., Towards greener and more sustainable batteries for electrical energy storage. *Nature Chemistry* **2014,** *7*, 19.
10. Görlin, M.; Halldin Stenlid, J.; Koroidov, S.; Wang, H.-Y.; Börner, M.; Shipilin, M.; Kalinko, A.; Murzin, V.; Safonova, O. V.; Nachtegaal, M.; Uheida, A.; Dutta, J.; Bauer, M.; Nilsson, A.; Diaz-Morales, O., Key activity descriptors of nickel-iron oxygen evolution electrocatalysts in the presence of alkali metal cations. *Nature communications* **2020,** *11* (1), 6181.
11. Kameda, Y.; Maeda, S.; Amo, Y.; Usuki, T.; Ikeda, K.; Otomo, T., Neutron Diffraction Study on the Structure of Hydrated Li+ in Dilute Aqueous Solutions. *The Journal of Physical Chemistry B* **2018,** *122* (5), 1695-1701.
12. Oncsik, T.; Trefalt, G.; Borkovec, M.; Szilagyi, I., Specific Ion Effects on Particle Aggregation Induced by Monovalent Salts within the Hofmeister Series. *Langmuir* **2015,** *31* (13), 3799-3807.
13. Morag, J.; Dishon, M.; Sivan, U., The Governing Role of Surface Hydration in Ion Specific Adsorption to Silica: An AFM-Based Account of the Hofmeister Universality and Its Reversal. *Langmuir* **2013,** *29* (21), 6317-6322.
14. Dye, J. L.; Nandi, P.; Jackson, J. E.; Lefenfeld, M.; Bentley, P. A.; Dunyak, B. M.; Kwarcinski, F. E.; Spencer, C. M.; Lindman, T. N.; Lambert, P.; Jacobson, P. K.; Redko, M. Y., Nano-Structures and Interactions of Alkali Metals within Silica Gel. *Chemistry of Materials* **2011,** *23* (9), 2388-2397.
15. Ducker, W. A.; Senden, T. J.; Pashley, R. M., Direct measurement of colloidal forces using an atomic force microscope. *Nature* **1991,** *353* (6341), 239-241.

16. Lee, S. S.; Fenter, P.; Nagy, K. L.; Sturchio, N. C., Real-time observation of cation exchange kinetics and dynamics at the muscovite-water interface. *Nat. Commun.* **2017,** *8* (1), 15826.
17. Trefalt, G.; Behrens, S. H.; Borkovec, M., Charge Regulation in the Electrical Double Layer: Ion Adsorption and Surface Interactions. *Langmuir* **2016,** *32* (2), 380-400.
18. Panse, K. S.; Wu, H.; Zhou, S.; Zhao, F.; Aluru, N. R.; Zhang, Y., Innermost Ion Association Configuration Is a Key Structural Descriptor of Ionic Liquids at Electrified Interfaces. *J. Phys. Chem. Lett.* **2022,** *13*, 9464-72.
19. Nakouzi, E.; Stack, A. G.; Kerisit, S. N.; Legg, B. A.; Mundy, C. J.; Schenter, G. K.; Chun, J.; De Yoreo, J. J., Moving beyond the Solvent-Tip Approximation to Determine Site-Specific Variations of Interfacial Water Structure through 3D Force Microscopy. *J. Phys. Chem. C* **2020,** *125*, 1282-91.
20. Wang, K.; Siboulet, B.; Rébiscoul, D.; Dufrêche, J.-F., How Ion Pair Formation Drives Adsorption in the Electrical Double Layer: Molecular Dynamics of Charged Silica–Water Interfaces in the Presence of Divalent Alkaline Earth Ions. *The Journal of Physical Chemistry C* **2021,** *125* (37), 20551-20569.
21. Piontek, S. M.; Dellostritto, M. J.; Mandal, B.; Marshall, T.; Klein, M. L.; Borguet, E., Probing Heterogeneous Charge Distributions at the α-Al2O3(0001)/H2O Interface. *J. Am. Chem. Soc.* **2020,** *142*, 12096-105.
22. Chen, S.-H.; Singer, S. J., Molecular Dynamics Study of the Electric Double Layer and Nonlinear Spectroscopy at the Amorphous Silica–Water Interface. *J. Phys. Chem. B* **2019,** *123* (29), 6364-6384.
23. Dewan, S.; Carnevale, V.; Bankura, A.; Eftekhari-Bafrooei, A.; Fiorin, G.; Klein, M. L.; Borguet, E., Structure of Water at Charged Interfaces: A Molecular Dynamics Study. *Langmuir* **2014,** *30*, 8056-65.
24. Porus, M.; Labbez, C.; Maroni, P.; Borkovec, M., Adsorption of monovalent and divalent cations on planar water-silica interfaces studied by optical reflectivity and Monte Carlo simulations. *The Journal of Chemical Physics* **2011,** *135* (6), 064701.
25. Grenoble, Z.; Baldelli, S., Adsorption of Benzyldimethylhexadecylammonium Chloride at the Hydrophobic Silica–Water Interface Studied by Total Internal Reflection Raman Spectroscopy: Effects of Silica Surface Properties and Metal Salt Addition. *The Journal of Physical Chemistry B* **2013,** *117* (34), 9882-9894.
26. Ma, E.; Geiger, F. M., Divalent Ion Specific Outcomes on Stern Layer Structure and Total Surface Potential at the Silica:Water Interface. *J. Phys. Chem. A* **2021,** *125* (46), 10079-10088.
27. Boamah, M. D.; Ohno, P. E.; Lozier, E.; Van Ardenne, J.; Geiger, F. M., Specifics about Specific Ion Adsorption from Heterodyne-Detected Second Harmonic Generation. *J. Phys. Chem. B* **2019,** *123* (27), 5848-5856.
28. Darlington, A. M.; Gibbs-Davis, J. M., Bimodal or Trimodal? The Influence of Starting pH on Site Identity and Distribution at the Low Salt Aqueous/Silica Interface. *The Journal of Physical Chemistry C* **2015,** *119* (29), 16560-16567.
29. Ma, E.; Ohno, P. E.; Kim, J.; Liu, Y.; Lozier, E. H.; Miller, T. F.; Wang, H.-F.; Geiger, F. M., A New Imaginary Term in the Second-Order Nonlinear Susceptibility from Charged Interfaces. *The Journal of Physical Chemistry Letters* **2021,** *12* (24), 5649-5659.
30. Boamah, M. D.; Ohno, P. E.; Lozier, E.; Van Ardenne, J.; Geiger, F. M., Specifics about Specific Ion Adsorption from Heterodyne-Detected Second Harmonic Generation. *Journal of Physical Chemistry B* **2019,** *123* (27), 5848-5856.

31. Luetzenkirchen, J.; Scharnweber, T.; Ho, T. A.; Striolo, A.; Sulpizi, M.; Abdelmonem, A., A set-up for simultaneous measurement of second harmonic generation and streaming potential and some test applications. *J. Coll. Int. Sci.* **2018,** *529*, 294-305.
32. van Spronsen, M. A.; Zhao, X.; Jaugstetter, M.; Escudero, C.; Duchoň, T.; Hunt, A.; Waluyo, I.; Yang, P.; Tschulik, K.; Salmeron, M. B., Interface Sensitivity in Electron/Ion Yield X-ray Absorption Spectroscopy: The TiO_2–H_2O Interface. *The Journal of Physical Chemistry Letters* **2021,** *12* (41), 10212-10217.
33. Karunaratne, W. V.; Sharma, S.; Ocko, B. M.; Margulis, C. J., Structure of Molten Alkali Chlorides at Charged Interfaces and the Prediction and Interpretation of Their X-ray Reflectivity. *The Journal of Physical Chemistry C* **2021,** *125* (45), 25227-25242.
34. Wood, K. N.; Teeter, G., XPS on Li-Battery-Related Compounds: Analysis of Inorganic SEI Phases and a Methodology for Charge Correction. *ACS Applied Energy Materials* **2018,** *1* (9), 4493-4504.
35. Bellucci, F.; Lee, S. S.; Kubicki, J. D.; Bandura, A.; Zhang, Z.; Wesolowski, D. J.; Fenter, P., Rb+ Adsorption at the Quartz(101)–Aqueous Interface: Comparison of Resonant Anomalous X-ray Reflectivity with ab Initio Calculations. *The Journal of Physical Chemistry C* **2015,** *119* (9), 4778-4788.
36. Dellostritto, M. J.; Kubicki, J.; Sofo, J. O., Density functional theory simulation of hydrogen-bonding structure and vibrational densities of states at the quartz (1 0 1)-water interface and its relation to dissolution as a function of solution pH and ionic strength. *Journal of Physics: Condensed Matter* **2014,** *26* (24), 244101.
37. Duval, Y.; Mielczarski, J. A.; Pokrovsky, O. S.; Mielczarski, E.; Ehrhardt, J. J., Evidence of the Existence of Three Types of Species at the Quartz-Aqueous Solution Interface at pH 0-10: XPS Surface Group Quantification and Surface Complexation Modeling. *J. Phys. Chem. B.* **2002,** *106* (11), 2937-2945.
38. Lyklema, J., *Fundamentals of Interface and Colloid Science*. Elsevier: 2000.
39. Langmuir, D., *Aqueous Environmental Chemistry*. Prentice Hall: Upper Saddle River, NJ 1997.
40. Stumm, W.; Morgan, J. J., *Aquatic Chemistry*. John Wiley & Sons, Inc.: New York, 1996; Vol. 3rd ed.
41. Bousse, L.; De Rooij, N. F.; Bergveld, P., Operation of Chemically Sensitive Field-Effect Sensors As a Function of the Insulator-Electrolyte Interface. *IEEE Trans. Electron Devices* **1983,** *ED-30*, 1263-70.
42. Khan, B.; Burgess, R. M.; Cantwell, M. G., Occurrence and Bioaccumulation Patterns of Per- and Polyfluoroalkyl Substances (PFAS) in the Marine Environment. *ACS ES&T Water Review* **2023,** *3*, 1243*1259.
43. Jia, Y. P.; Shi, K.; Liao, J. F.; Peng, J. R.; Hao, Y.; Qu, Y.; Chen, L. J.; Liu, L.; Yuan, X.; Qian, Z. Y.; Wei, X. W., Effects of Cetyltrimethylammonium Bromide on the Toxicity of Gold Nanorods Both In Vitro and In Vivo: Molecular Origin of Cytotoxicity and Inflammation. *Small Methods* **2020,** *4* (3), 1900799.
44. Elfeky, S. A.; Mahmoud, S. E.; Youssef, A. F., Applications of CTAB modified magnetic nanoparticles for removal of chromium (VI) from contaminated water. *Journal of Advanced Research* **2017,** *8* (4), 435-443.
45. Joseph, D.; Rodriguez, R. D.; Verma, A.; Pousaneh, E.; Zahn, D. R. T.; Lang, H.; Chandra, S., Electrochemistry and surface-enhanced Raman spectroscopy of CTAB modulated interactions of magnetic nanoparticles with biomolecules. *RSC Advances* **2017,** *7* (7), 3628-3634.

46. Wan, J.; Wang, J.-H.; Liu, T.; Xie, Z.; Yu, X.-F.; Li, W., Surface chemistry but not aspect ratio mediates the biological toxicity of gold nanorods in vitro and in vivo. *Scientific Reports* **2015,** *5* (1), 11398.
47. Zhang, Y.; Newton, B.; Lewis, E.; Fu, P. P.; Kafoury, R.; Ray, P. C.; Yu, H., Cytotoxicity of organic surface coating agents used for nanoparticles synthesis and stability. *Toxicology in Vitro* **2015,** *29* (4), 762-768.
48. Wu, H.; Li, Z.; Wang, Y.; Zhu, W., Surface Decoration of Cetyltrimethyl Ammonium Bromide on SiC Particles and Its Effects on the Co-Deposition Process. *The Journal of Physical Chemistry B* **2021,** *125* (18), 4874-4882.
49. Li, R.; Wang, Z.; Gu, X.; Chen, C.; Zhang, Y.; Hu, D., Study on the Assembly Structure Variation of Cetyltrimethylammonium Bromide on the Surface of Gold Nanoparticles. *ACS Omega* **2020,** *5* (10), 4943-4952.
50. Tsagkaropoulou, G.; Allen, F. J.; Clarke, S. M.; Camp, P. J., Self-assembly and adsorption of cetyltrimethylammonium bromide and didodecyldimethylammonium bromide surfactants at the mica–water interface. *Soft Matter* **2019,** *15* (41), 8402-8411.
51. Hayes, P. L.; Keeley, A. R.; Geiger, F. M., Structure of the Cetyltrimethylammonium Surfactant at Fused Silica/Aqueous Interfaces Studied by Vibrational Sum Frequency Generation. *The Journal of Physical Chemistry B* **2010,** *114* (13), 4495-4502.
52. Tyrode, E.; Rutland, M. W.; Bain, C. D., Adsorption of CTAB on Hydrophilic Silica Studied by Linear and Nonlinear Optical Spectroscopy. *J. Am Chem. Soc.* **2008,** *130* (51), 17434-17445.
53. Ohno, P. E.; Chang, H.; Spencer, A. P.; Liu, Y.; Boamah, M. D.; Wang, H. F.; Geiger, F. M., Beyond the Gouy-Chapman Model with Heterodyne-Detected Second Harmonic Generation. *J. Phys. Chem. Lett.* **2019,** *10* (10), 2328.
54. Chang, H.; Ohno, P. E.; Liu, Y.; Lozier, E. H.; Dalchand, N.; Geiger, F. M., Direct Measurement of Charge Reversal on Lipid Bilayers Using Heterodyne-Detected Second Harmonic Generation Spectroscopy. *The Journal of Physical Chemistry B* **2020,** *124* (4), 641-649.
55. Boamah, M. D.; Ohno, P. E.; Lozier, E.; van Ardenne, J.; Geiger, F. M., Specifics About Specific Ion Adsorption from Heterodyne-Detected Second Harmonic Generation. **2019,** *ChemRxiv.Preprint*.
56. Hore, D. K.; Tyrode, E. C., Probing Charged Aqueous Interfaces Near Critical Angles: Effect of Varying Coherence Length. *The Journal of Physical Chemistry C* **2019,** *123* (27), 16911-20.
57. Ohno, P. E.; Chang, H.; Spencer, A. P.; Liu, Y.; Boamah, M. D.; Wang, H.-f.; Geiger, F. M., Beyond the Gouy–Chapman Model with Heterodyne-Detected Second Harmonic Generation. *J. Phys. Chem. Lett.* **2019,** *10* (10), 2328-2334.
58. Ohno, P. E.; Wang, H.-f.; Paesani, F.; Skinner, J. L.; Geiger, F. M., Second-Order Vibrational Lineshapes from the Air/Water Interface. *J. Phys. Chem. A* **2018,** *122* (18), 4457-4464.
59. Pezzotti, S.; Galimberti, D. R.; Shen, Y. R.; Gaigeot, M.-P., What the Diffuse Layer (DL) Reveals in Non-Linear SFG Spectroscopy. *Minerals* **2018,** *8* (7), 305.
60. Ohno, P. E.; Wang, H.-f.; Geiger, F. M., Second-order spectral lineshapes from charged interfaces. *Nature communications* **2017,** *8* (1), 1032.
61. Gonella, G.; Lütgebaucks, C.; de Beer, A. G. F.; Roke, S., Second Harmonic and Sum Frequency Generation from Aqueous Interfaces is Modulated by Interference. *The Journal of Physical Chemistry C* **2016,** *120* (17), 9165-9173.

62. Ohno, P. E.; Saslow, S. A.; Wang, H.-f.; Geiger, F. M.; Eisenthal, K. B., Phase-referenced Nonlinear Spectroscopy of the alpha-Quartz/Water Interface. *Nature communications* **2016,** *7*, 13587.
63. Wen, Y.-C.; Zha, S.; Liu, X.; Yang, S.; Guo, P.; Shi, G.; Fang, H.; Shen, Y. R.; Tian, C., Unveiling Microscopic Structures of Charged Water Interfaces by Surface-Specific Vibrational Spectroscopy. *Physical Review Letters* **2016,** *116* (1), 016101.
64. Ma, E.; Ohno, P. E.; Kim, K.; Liu, Y.; Lozier, E. H.; Miller III, T. F.; Wang, H.-f.; Geiger, F. M., A New Imaginary Term in the 2nd Order Nonlinear Susceptibility from Charged Interfaces. *J. Phys. Chem. Lett.* **2021,** *12* (24), 5649-59.
65. Yamaguchi, S.; Shiratori, K.; Morita, A.; Tahara, T., Electric quadrupole contribution to the nonresonant background of sum frequency generation at air/liquid interfaces. *The Journal of Chemical Physics* **2011,** *134* (18), 184705.
66. Wei, X.; Hong, S.-C.; Lvovsky, A. I.; Held, H.; Shen, Y. R., Evaluation of Surface vs Bulk Contributions in Sum-Frequency Vibrational Spectroscopy Using Reflection and Transmission Geometries. *The Journal of Physical Chemistry B* **2000,** *104* (14), 3349-3354.
67. Garcia Rey, N.; Weissenborn, E.; Schulze-Zachau, F.; Gochev, G.; Braunschweig, B., Quantifying Double-Layer Potentials at Liquid–Gas Interfaces from Vibrational Sum-Frequency Generation. *J. Phys. Chem. C* **2019,** *123* (1279-86).
68. Shen, Y. R., *The Principles of Nonlinear Optics*. John Wiley & Sons, Inc.: Hoboken, NJ, 2003.
69. Dalstein, L.; Chiang, K.-Y.; Wen, Y.-C., Direct Quantification of Water Surface Charge by Phase-Sensitive Second Harmonic Spectroscopy. *The Journal of Physical Chemistry Letters* **2019,** *10* (17), 5200-5205.
70. Lütgebaucks, C.; Gonella, G.; Roke, S., Optical label-free and model-free probe of the surface potential of nanoscale and microscopic objects in aqueous solution. *Phys. Rev. B* **2016,** *94* (19), 195410.
71. Ohno, P. E.; Saslow, S. A.; Wang, H.; Geiger, F. M.; Eisenthal, K. B., Phase referenced nonlinear spectroscopy of the alpha-quartz/water interface. *Nat. Commun.* **2016,** *7*, 13587.
72. Rehl, B.; Ma, E.; Parshotam, S.; DeWalt-Kerian, E. L.; Liu, T.; Geiger, F. M.; Gibbs, J. M., Water Structure in the Electrical Double Layer and the Contributions to the Total Interfacial Potential at Different Surface Charge Densities. *Journal of the American Chemical Society* **2022,** *144* (36), 16338-16349.
73. Duval, Y.; Mielczarski, J. A.; Pokrovsky, O. S.; Mielczarski, E.; Ehrhardt, J. J., Evidence of the Existence of Three Types of Species at the Quartz−Aqueous Solution Interface at pH 0−10: XPS Surface Group Quantification and Surface Complexation Modeling. *J. Phys. Chem. B* **2002,** *106* (11), 2937-2945.
74. Rehl, B.; Rashwan, M.; DeWalt-Kerian, E. L.; Jarisz, T. A.; Darlington, A. M.; Hore, D. K.; Gibbs, J. M., New Insights into χ(3) Measurements: Comparing Nonresonant Second Harmonic Generation and Resonant Sum Frequency Generation at the Silica/Aqueous Electrolyte Interface. *The Journal of Physical Chemistry C* **2019,** *123* (17), 10991-11000.
75. Dreier, L. B.; Bernhard, C.; Gonella, G.; Backus, E. H. G.; Bonn, M., Surface Potential of a Planar Charged Lipid–Water Interface. What Do Vibrating Plate Methods, Second Harmonic and Sum Frequency Measure? *The Journal of Physical Chemistry Letters* **2018,** *9* (19), 5685-5691.
76. Ohno, P. E.; Saslow, S. A.; Wang, H.-f.; Geiger, F. M.; Eisenthal, K. B., Phase-referenced nonlinear spectroscopy of the α-quartz/water interface. *Nat. Commun.* **2016,** *7*, 13587.

77. Yan, E. C. Y.; Liu, Y.; Eisenthal, K. B., New Method for Determination of Surface Potential of Microscopic Particles by Second Harmonic Generation. *J. Phys. Chem. B* **1998,** *102* (33), 6331-6336.
78. Zhao, X.; Ong, S.; Wang, H.; Eisenthal, K. B., New method for determination of surface pKa using second harmonic generation. *Chem. Phys. Lett.* **1993,** *214* (2), 203-207.
79. Bard, A. J.; Faulkner, L. R., *Electrochemical Methods: Fundamentals and Applications*. 2nd ed.; John Wiley and Sons: New York, 2000.
80. Diot, J. L.; Joseph, J.; Martin, J. R.; Clechet, P., pH Dependence of the Si/SiO2 Interface State Density for EOS Systems: Quasi-Static and AC Conductance Methods. *J. Electroanal. Chem.* **1985,** *193*, 75-88.
81. Brown, M. A.; Abbas, Z.; Kleibert, A.; Green, R. G.; Goel, A.; May, S.; Squires, T. M., Determination of Surface Potential and Electrical Double-Layer Structure at the Aqueous Electrolyte-Nanoparticle Interface. *Phys. Rev. X* **2016,** *6*, 011007.
82. DeWalt-Kerian, E. L.; Kim, S.; Azam, M. S.; Zeng, H.; Liu, Q.; Gibbs, J. M., pH-Dependent Inversion of Hofmeister Trends in the Water Structure of the Electrical Double Layer. *The Journal of Physical Chemistry Letters* **2017,** *8* (13), 2855-2861.
83. Azam, M. S.; Darlington, A.; Gibbs-Davis, J. M., The Influence of Concentration on Specific Ion Effects at the Silica/Water Interface. *Journal of Physics: Condensed Matter* **2014,** *26* (24), 244107.
84. Azam, M. W.; Weeraman, C. N.; Gibbs-Davis, J. M., Specific cation effects on the bimodal acid-base behavior of the silica/water interface. *J. Phys. Chem. Lett.* **2012,** *3*, 1269-74.
85. Flores, S. C.; Kherb, J.; Konelick, N.; Chen, X.; Cremer, P. S., The Effects of Hofmeister Cations at Negatively Charged Hydrophilic Surfaces. *J. Phys. Chem. C* **2012,** *116*, 5730-34.
86. Levine, B. F.; Bethea, C. G., Effects on hyperpolarizabilities of molecular interactions in associating liquid mixtures. *Journal of Chemical Physics* **1976,** *65* (6), 2429-38.
87. Gubskaya, A. V.; Kusalik, P. G., The multipole polarizabilities and hyperpolarizabilities of the water molecule in liquid state: an ab initio study. *Mol. Phys.* **2001,** *99*, 1107-20.
88. Maroulis, G., Hyperpolarizability of H2O. *J. Chem. Phys.* **1991,** *94*, 1182-90.
89. Fumagalli, L.; Esfandiar, A.; Fabregas, R.; Hu, S.; Ares, P.; Janardanan, A.; Yang, Q.; Radha, B.; Taniguchi, T.; Watanabe, K.; Gomila, G.; Novoselov, K. S.; Geim, A. K., Anomalously low dielectric constant of confined water. *Science* **2018,** *360*, 1339-42.
90. Skoog, D. A.; Holler, F. J.; Crouch, S. R., *Principles of Instrumental Analysis*. 7 ed.; Cengage Learning: Boston, MA, 2017.
91. Gmür, T. A.; Goel, A.; Brown, M. A., Quantifying Specific Ion Effects on the Surface Potential and Charge Density at Silica Nanoparticle–Aqueous Electrolyte Interfaces. *J. Phys. Chem. C* **2016,** *120*, 16617-16625.
92. Dove, P. M.; Craven, C. M., Surface charge density on silica in alkali and alkaline earth chloride electrolyte solutions. *Geochm. Cosmochim. Acta* **2005,** *69*, 4963-70.
93. Parshotam, S.; Zhang, W.; Rehl, B.; Darlington, A.; Sikder, M. D. H.; Brown, A.; Gibbs, J. M., Revealing Silica's pH-Dependent Second Harmonic Generation
Response with Overcharging. *J. Phys. Chem. C* **2013,** *127*, 8389-98.
94. Kirkham, M. B., Structure and Properties of Water. In *Principles of Soil and Plant Water Relations*, Kirkham, M. B., Ed. Academic Press: Burlington, 2005.
95. Petrenko, V. F.; Whitworth, R. W., *Physics of Ice*. Oxford University Press: New York, 1999.

96. Hayes, P. L.; Chen, E. H.; Achtyl, J. L.; Geiger, F. M., An Optical Voltmeter for Studying Cetyltrimethylammonium Interacting with Fused Silica/Aqueous Interfaces at High Ionic Strengthâ€ *Journal of Physical Chemistry A* **2009,** *113* (16), 4269-4280.
97. Chang, H.; Ohno, P. E.; Liu, L.; Geiger, F. M., Direct Measurement of Charge Reversal on Lipid Bilayers using Heterodyne-Detected Second Harmonic Generation Spectroscopy. *J. Phys. Chem. B* **2020,** *124* (641-9).
98. Abdelmonem, A.; Zhang, Y.; Braunschweig, B.; Glikman, D.; Rumpel, A.; Peukert, W.; Begović, T.; Liu, X.; Lützenkirchen, J., Adsorption of CTAB on Sapphire-c at High pH: Surface and Zeta Potential Measurements Combined with Sum-Frequency and Second-Harmonic Generation. *Langmuir* **2022,** *38* (11), 3380-3391.
99. Nguyen, K. T.; Nguyen, A. V.; Evans, G. M., Interfacial Water Structure at Surfactant Concentrations below and above the Critical Micelle Concentration as Revealed by Sum Frequency Generation Vibrational Spectroscopy. *The Journal of Physical Chemistry C* **2015,** *119* (27), 15477-15481.
100. Torres, L. L.; Chauveau, M.; Hayes, P. L., Macromolecular Structure of Dodecyltrimethylammonium Chloride at the Silica/Water Interface Studied by Sum Frequency Generation Spectroscopy. *The Journal of Physical Chemistry C* **2015,** *119* (42), 23917-23927.
101. Abdelmonem, A.; Zhang, Y.; Braunschweig, B.; Glikman, D.; Rumpel, A.; Peukert, W.; Begovic, T.; Liu, X.; Luetzenkirchen, J., Adsorption of CTAB on Sapphire-c at High pH: Surface and Zeta Potential Measurements Combined with Sum-Frequency and Second-Harmonic Generation. *Langmuir* **2022,** *38*, 3380-91.

Table I. Table of solution conditions surveyed. M = alkali cation.

pH	[MCl] mM	Species
2	100	MCl + HCl
5.8	1	MCl
5.8	100	MCl
10	100	MCl + MOH
13	1000	MCl + MOH
14	1000	MOH
5.8	1	CTAB
4.6	0.02	PFOA
5.9	0.02	PFOS

Figure Captions

Figure 1. Summary of $\chi^{(2)}$ and $\Phi(0)$ obtained at indicated pH and alkali chloride concentrations. Error bars were obtained by propagating the standard deviation of the mean of the fit parameters (see Section II. C) from four replicate fringe measurements at the aqueous phase conditions indicated.

Figure 2. (top) Point estimates of $\Delta\chi^{(2)}$ obtained by subtracting from the $\chi^{(2)}$ values shown in Fig. 1 the $\chi^{(2)}$ values of the silica:water interface held at pH 2 for all five salts studied. (2nd from top) Point estimates of the number of net-aligned water molecules in the Stern layer at conditions indicated. (3rd from top) Point estimate of the second-order nonlinear susceptibility associated with the ions in the interfacial region at elevated pH. (bottom) Free energy density point estimates associated with net water alignment in the Stern layer at conditions indicated. Error bars were obtained by propagating the standard deviation of the mean of the fit parameters (see Section II. C) from four replicate fringe measurements at the aqueous phase conditions indicated.

Figure 3. (A) $\Phi(0)$ and $\chi^{(2)}$ of 1 mM alkali metals, 1 mM CTAB, and 20 μM PFOA and PFOS at the conditions indicated in Table I. (B) SHG interference fringes of 1 mM RbCl (red) and 1 mM CTAB (grey) relative to pure water (blue). For each fringe pair, a difference of 1 mm on the abscissa corresponds to a phase change of 3.16°.

Figure 1.

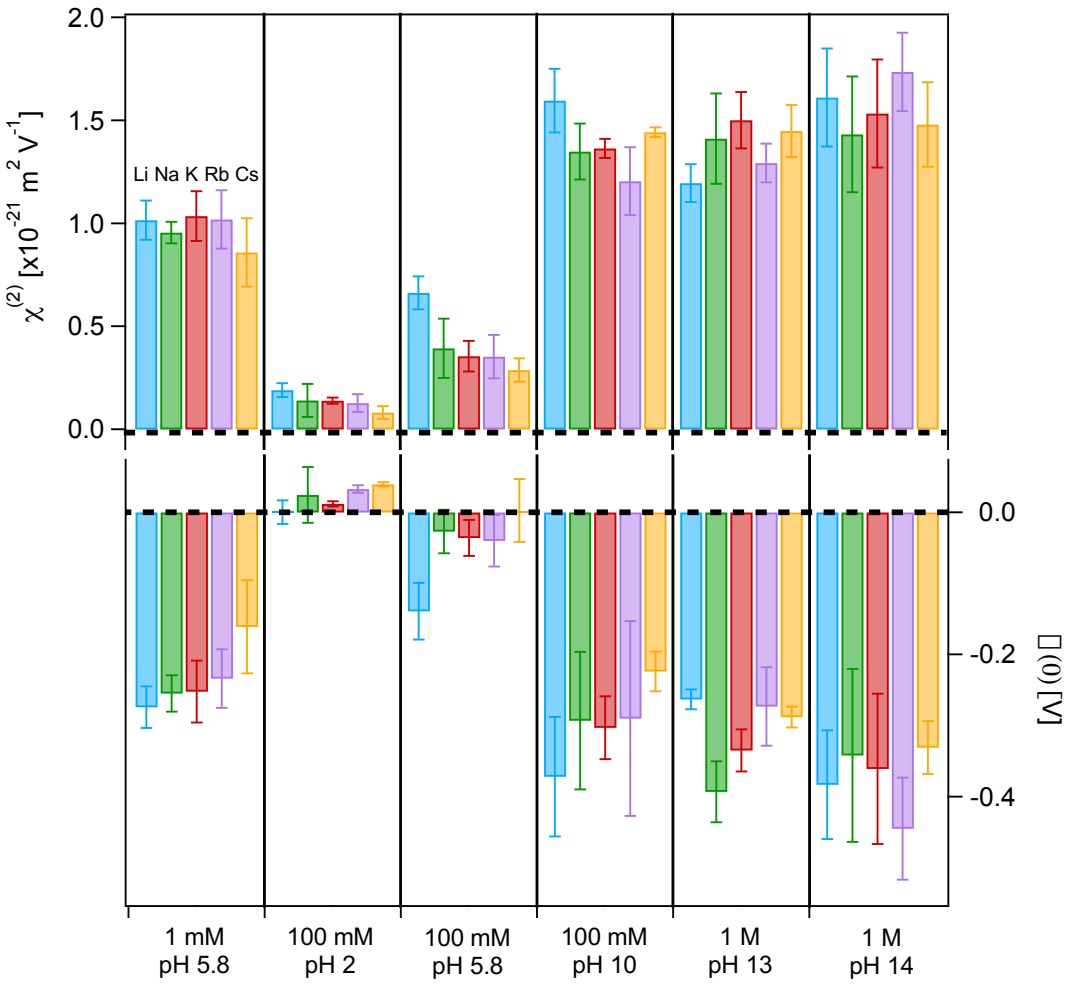
2.0
1.5
1.0
0.5
0.0
Li Na K Rb Cs
χ(2) [x10-21 m2 V-1]
0.0
-0.2
-0.4
□(0) [V]
1 mM pH 5.8
100 mM pH 2
100 mM pH 5.8
100 mM pH 10
1 M pH 13
1 M pH 14

Figure 2.

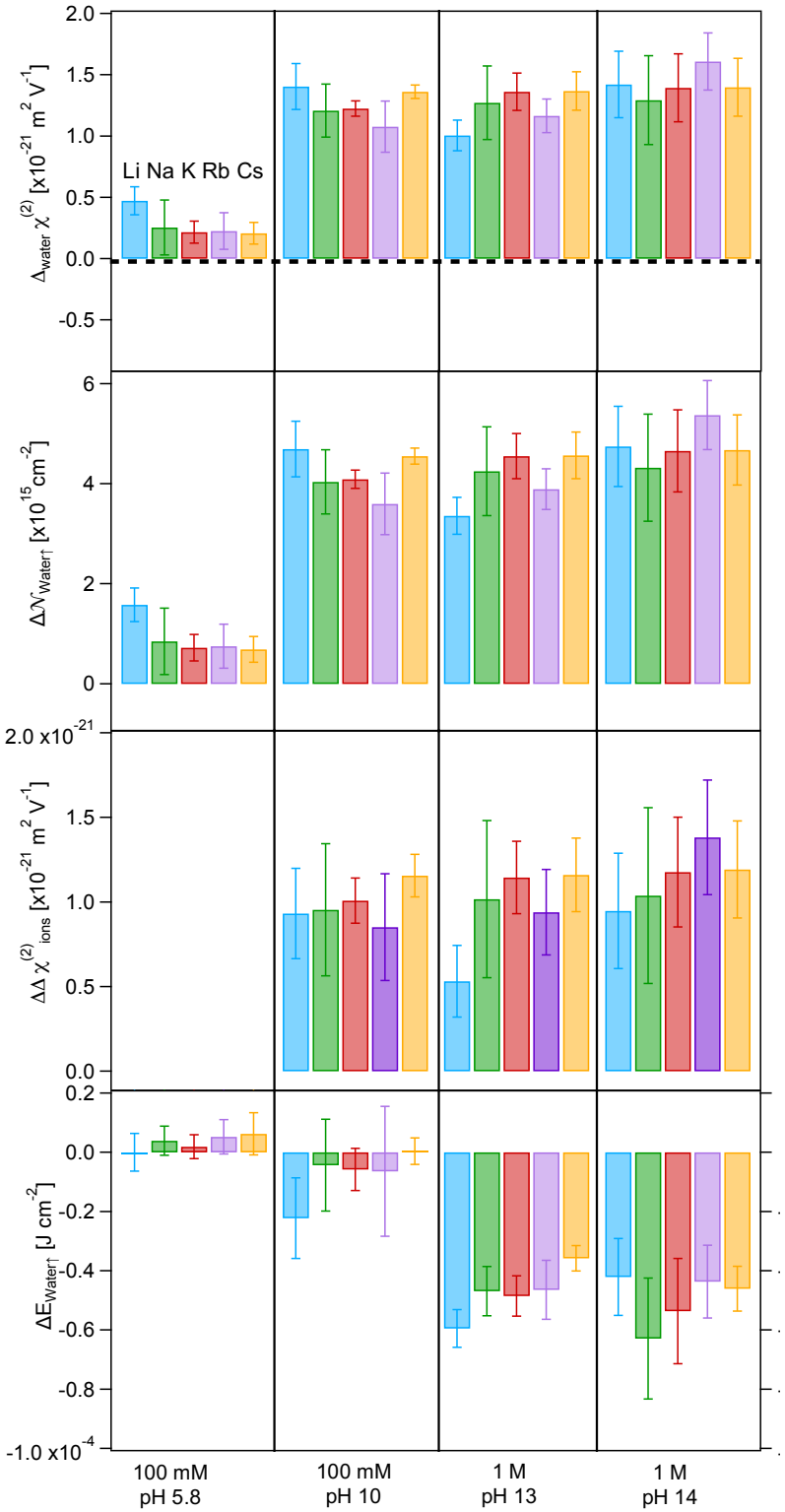
Li Na K Rb Cs
$\Delta_{water}\chi^{(2)}$ [x10^{-21} m^2 V^{-1}]
$\Delta N_{Water\uparrow}$ [x10^{15} cm^{-2}]
$\Delta\Delta\chi^{(2)}_{ions}$ [x10^{-21} m^2 V^{-1}]
$\Delta E_{Water\uparrow}$ [J cm^{-2}]
100 mM pH 5.8
100 mM pH 10
1 M pH 13
1 M pH 14

Figure 3.

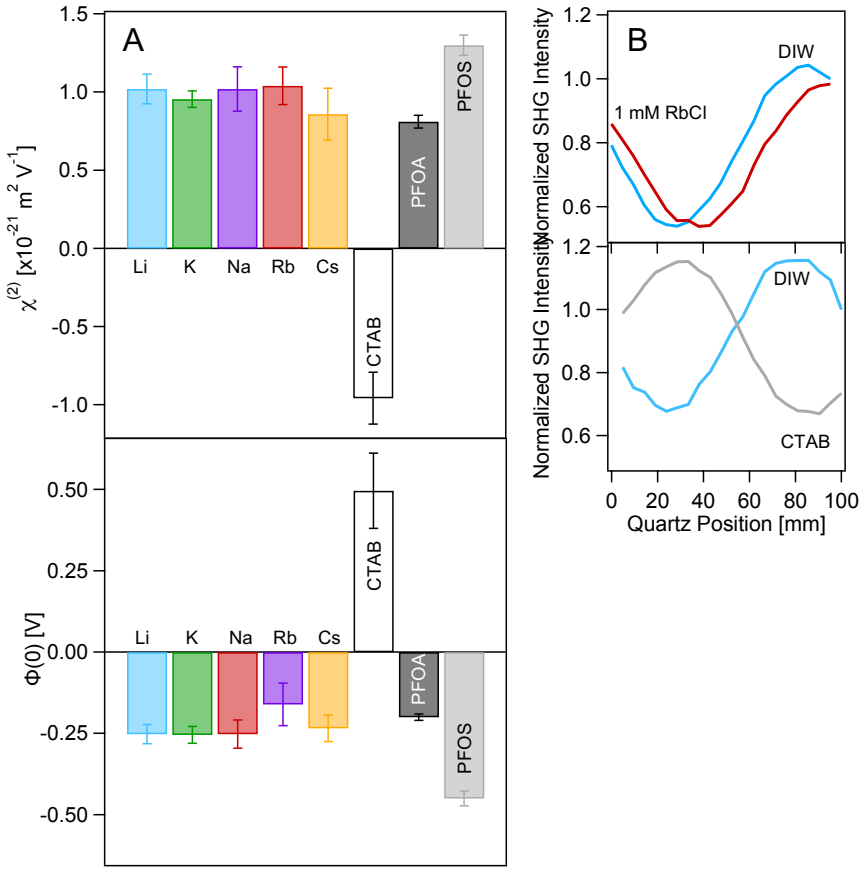
A
B
Li
K
Na
Rb
Cs
CTAB
PFOA
PFOS
1 mM RbCl
DIW
Quartz Position [mm]
Normalized SHG Intensity

TOC Graphic

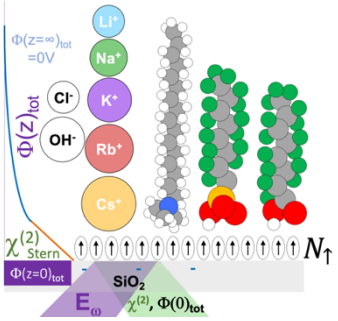
Li+
Na+
K+
Rb+
Cs+
Cl-
OH-
Φ(z=∞)tot =0V
Φ(z)tot
χ(2) Stern
Φ(z=0)tot
SiO2
Eω
χ(2), Φ(0)tot
N↑